Supporting Information

Studies on the Photoelectronic Properties of Manganese (Mn)-doped Lead-free Double Perovskite

Shaoming Xue,[1] Qiaoqian Wu,[1] Qiuhong Huo,[1,2] Jun Mi,[1,2] ChengBo Guan,[1] Wei-Yan Cong,[1] Zhenkui Zhang[3] and Junfeng Ren[4] Ying-Bo Lu,[1,2,a)]

[1] School of Space Science and Physics, Shandong University, Weihai 264209, China

[2] Physical-Chemical Materials Analytical & Testing Center, Shandong University, Weihai 264209, China

[3] School of Science, Langfang Normal University, Langfang 065000, China

[4] School of Physics and Electronics, Shandong Normal University, Jinan 250014, China

[a)] Author to whom correspondence should be addressed.

Electronic mail: lyb@sdu.edu.cn.

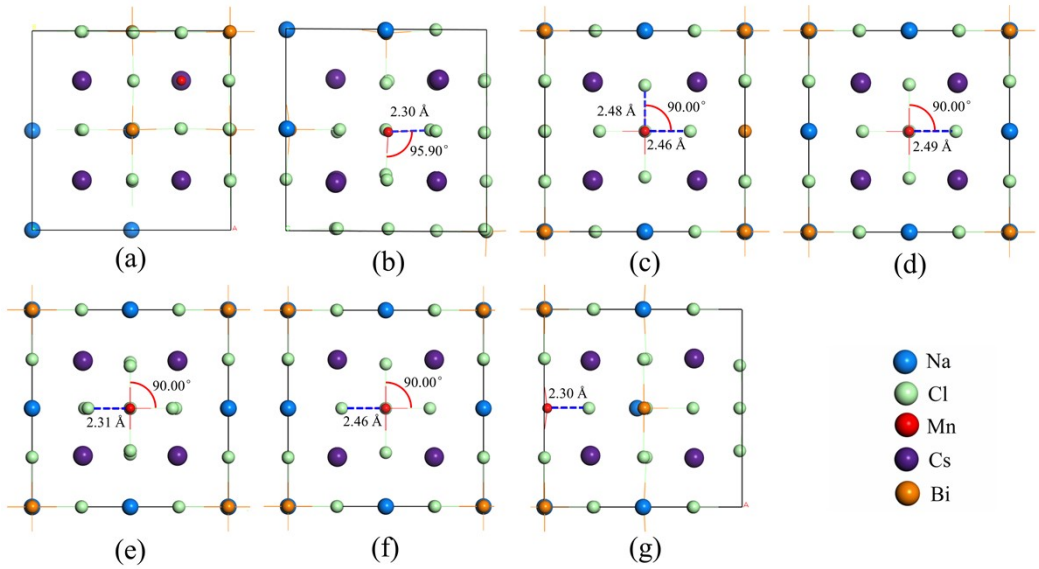

Figure S1. Geometric structures of $Cs_2NaBiCl_6$ containing the (a) Mn_{Cs} defects (b) $Mn_{Na}V_{Cs}$ defects (c) $Mn_{Na}V_{Na}$ defects (d) $Mn_{Na}Mn_{Bi}$ defects (local structure of Mn_{Na} in $Mn_{Na}Mn_{Bi}$ defects) (e) $Mn_{Na}Mn_{Bi}$ defects (local structure of Mn_{Bi} in $Mn_{Na}Mn_{Bi}$ defects) (f) Mn_{Na} defects (g) $Mn_{Bi}V_{Cl}$ defects, respectively.

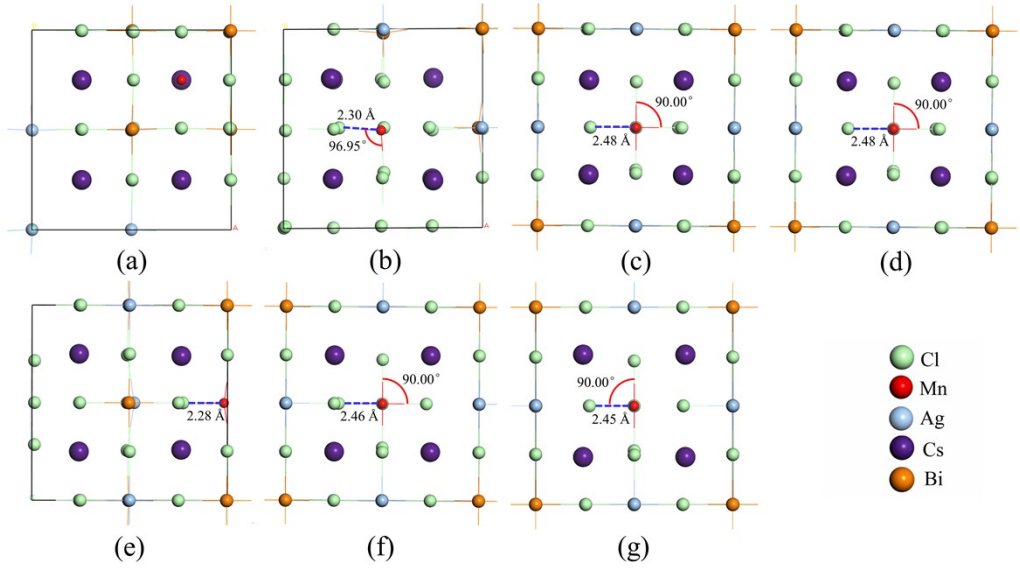

Figure S2. Geometric structures of $Cs_2AgBiCl_6$ containing the (a) Mn_{Cs} defects (b) $Mn_{Ag}V_{Cs}$ defects (c) $Mn_{Ag}Mn_{Bi}$ defects (local structure of Mn_{Ag} in $Mn_{Ag}Mn_{Bi}$ defects) (d) $Mn_{Ag}Mn_{Bi}$ defects (local structure of Mn_{Bi} in $Mn_{Ag}Mn_{Bi}$ defects) (e) $Mn_{Bi}V_{Cl}$ defects (f) Mn_{Ag} defects (g) $Mn_{Ag}V_{Ag}$ defects, respectively.

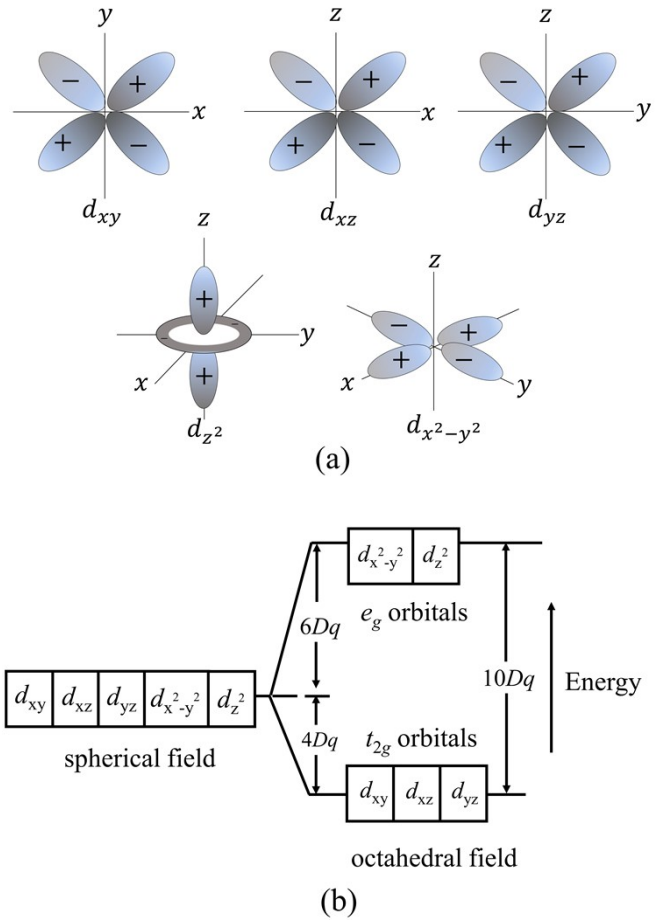

Figure S3. Scheme to describe the splitting of *d*-orbital from the (a) spherical to the (b) octahedral crystal field, respectively, as a result of the interaction of metal orbitals with ligand orbitals.

Table S1. Calculated IpCOHP in $Cs_2NaBiCl_6:Mn^{2+}$ and $Cs_2AgInCl_6:Mn^{2+}$ systems. The E_F represents the Fermi level.

		Distance (Å)	IpCOHP at E_F
$Cs_2NaBiCl_6:Mn^{2+}$	Cl6-Mn29	2.34	-2.10
	Cl10-Mn29	2.34	-2.10
	Cl14-Mn29	2.34	-2.04
	Cl18-Mn29	2.34	-2.04
	Cl22-Mn29	2.34	-1.98
	Cl26-Mn29	2.34	-1.98
	Ave. IpCOHP		-2.04
$Cs_2AgInCl_6:Mn^{2+}$	Cl6-Mn25	2.42	-1.66
	Cl13-Mn25	2.44	-1.62
	Cl14-Mn25	2.42	-1.66
	Cl15-Mn25	2.44	-1.62
	Cl16-Mn25	2.42	-1.72
	Cl17-Mn25	2.42	-1.72
	Ave. IpCOHP		-1.66

The detailed descriptions of computing the change in *Dq* and *B*, *C*

For $Cs_2NaBiCl_6$:Mn^{2+} systems, the PLE band peaking at ~ 297 nm and 358 nm are ascribed to the $^6A_1(^6S)$-$^4T_1(^4P)$ and $^6A_1(^6S)$-$^4T_2(^4D)$ transitions of Mn^{2+}, respectively. The orange-yellow PL peak at 577 nm is attributed to the $^4T_1(^4G)$-$^6A_1(^6S)$ transitions of Mn^{2+}. The equation (2), (3) and (5) in the main text can change to:

$$7B + 7C = \frac{10^7}{297} \qquad (6)$$

$$17B + 5C = \frac{10^7}{358} \qquad (7)$$

$$E_2 = \frac{10^7}{577} \qquad (8)$$

Connecting equations (6) and (7) above, we can obtain *B* and *C* are 324 cm^{-1} and 4486cm^{-1}, respectively. The equation (4) in the main text can be simplified as:

$$Dq = \{\left[\frac{36B^2(E_2 - 10B - 5C)}{19B + 7C - E_2} + (10B + 7C - E_2)(10B + 5C - E_2)\right]\frac{1}{100}\}^{\frac{1}{2}} \qquad (9)$$

Taking the values of E_2, *B* and *C* into the equation (9), then *Dq* = 1195 cm^{-1} is acquired. Thus, we obtain *B* = 324 cm^{-1}, *C* = 4486 cm^{-1} and *Dq* = 1195 cm^{-1}, respectively.

For $Cs_2AgInCl_6$:Mn^{2+} systems, the calculation steps are similar to the details discussed above. Thus, the calculation results of the *B*, *C* and *Dq* are 509 cm^{-1}, 5071 cm^{-1} and =1895 cm^{-1}, respectively.

The detailed descriptions of how to draw the Tanabe-Sugano diagrams

We attach the original references about the Tanabe-Sugano diagrams for d^5 in here[1] (10.1143/JPSJ.9.766), which we draw Figure 8 in the manuscript by reference to this original literature.

1. Y. Tanabe and S. Sugano, *J. Phys. Soc. Japan*, 1954, **9**, 766-779.